Mixed Protein Blends Composed of Gelatin and *Bombyx mori* Silk Fibroin: Effects of Solvent-Induced Crystallization and Composition

Eun S. Gil,[†] David J. Frankowski,[‡] Michelle K. Bowman,[§] Arif O. Gozen,[‡] Samuel M. Hudson,*[,†] and Richard J. Spontak[‡,§]

Fiber and Polymer Science Program and Departments of Chemical and Biomolecular Engineering and Materials Science and Engineering, North Carolina State University, Raleigh, North Carolina 27695

Received August 29, 2005; Revised Manuscript Received December 5, 2005

Novel protein blends have been prepared by mixing gelatin (G) with *Bombyx mori* silk fibroin (SF) and using aqueous methanol (MeOH) to post-induce SF crystallization. When co-cast from solution, amorphous blends of these polymers appear homogeneous, as discerned from visual observation, microscopy, and Fourier-transform infrared (FTIR) spectroscopy. Upon subsequent exposure to aqueous MeOH, SF undergoes a conformational change from random coil to β sheet. This transformation occurs in pure SF, as well as in each of the G/SF blends, according to X-ray diffractometry and thermal calorimetry. The influence of MeOH-induced SF crystallization on structure and property development has been ascertained in terms of preparation history and blend composition. Thermal gravimetric analysis reveals that the presence of β sheets in SF and G/SF blends improves thermal stability, while extensional rheometry confirms that SF crystallization enhances the tensile properties of the blends. By preserving a support scaffold above the G helix-to-coil transition temperature, the formation of crystalline SF networks in G/SF blends can be used to stabilize G-based hydrogels for biomaterial and pharmaceutical purposes. The present study not only examines the properties of G/SF blends before and after SF crystallization, but also establishes the foundation for future research into thermally responsive G/SF bioconjugates.

Introduction

Silk fibroin (SF) derived from *Bombyx mori* is a fibrous protein composed of heavy (350 kDa) and light (25 kDa) polypeptide fractions connected by disulfide linkages. The high-molar-mass chains consist primarily of Gly-Ala-Gly-Ala-Ser residues and are responsible for the formation of crystalline β-sheet structures,[1] which are interspersed with amorphous regions rich in bulky amino acids. Once the sericin coating present in raw silk is removed, the resultant SF can be dissolved in neutral salt solutions such as LiBr and $Ca(NO_3)_2$.[2−4] Regenerated SF in film,[2] fiber,[3] and scaffold[4] form has been produced in this fashion for use as a biomaterial due to its good wet-state mechanical strength,[4] cell growth biocompatibility,[5] high dissolved-oxygen and water-vapor permeability,[6] and enzymatic degradation resistance.[7] Unlike native SF, though, regenerated SF adopts a random-coil conformation and is intrinsically amorphous.[2] When as-cast SF is immersed in a dehydrating solvent such as methanol (MeOH), crystallization can be induced as the SF chains undergo a transformation from random-coil to β-sheet conformation (silk II).[2,3] Because of its attractive properties, SF has recently been studied in blends with other (bio)macromolecules, such as chitosan,[8] cellulose,[9] poly(vinyl alcohol),[10] poly(acrylic acid),[11] and nylon-6,6.[12] Previous studies such as these have not, however, reported that exposing a blend containing SF to a solvent such as MeOH promotes SF crystallization. If the secondary β-sheet structure of SF could be controllably re-formed in blends of SF with other macromolecules, crystallizable interpenetrating networks (IPNs) or semi-IPNs could be designed complete with intrinsic physical cross-link sites, thereby precluding the need for chemical cross-linking agents.

To demonstrate the feasibility of using SF in this fashion, we have blended SF with another common protein, gelatin (G), which is obtained by breaking the triple-helix structure of collagen into single-stranded macromolecules through thermal denaturation or a combination of physical and chemical degradation. Due to its inherent biocompatibility and biodegradability, G is of considerable interest in the biomedical industry for use in drug capsules,[13] vascular prosthetic sealants,[14] wound dressing formulations,[15] and tissue engineering scaffolds.[16] An important property of G in aqueous solution is a thermally reversible conformational transition, which is responsible for inducing gelation (due to re-formation of some of the triple-helix structure to form a loose network) upon cooling from solution. At ambient temperature, G molecules form networks wherein the triple helices serve as physical cross-link sites. Upon heating to body temperature (~37 °C), the triple helices dissolve due to denaturation, and G again becomes fully soluble.[17] Thus, to stabilize the thermal and mechanical properties of G at elevated temperatures, cross-linking agents such as glutaraldehyde,[18] diisocyanates,[19] and carbodiimides[20] are commonly used to promote chemical cross-linking for long-term biomedical applications. Bigi et al.[21] have reported that genipin can also be used for this purpose with reduced cytotoxicity. Chemical cross-linking has nonetheless been shown[22] to have a deleterious effect on G: it reduces the mobility of G molecules, thereby eliminating the helix-to-coil transition. We have previously demonstrated[23,24] that, upon MeOH-induced crystallization, SF β-sheet networks stabilize G/SF hydrogels at elevated temper-

* To whom correspondence should be addressed. E-mail: Sam_Hudson@ncsu.edu.

[†] Fiber and Polymer Science Program.

[‡] Department of Chemical and Biomolecular Engineering.

[§] Department of Materials Science and Engineering.

10.1021/bm050622i CCC: $33.50
Published on Web 01/31/2006

atures and permit retention of the G helix-to-coil transition due to unconstrained molecular mobility.

In the present study, we examine pure SF and G, as well as G/SF blends varying in composition, with and without aqueous MeOH treatment to (i) establish the incidence of solvent-induced β-sheet formation and (ii) discern the effect of SF crystallization on morphological and property development in this novel family of materials.

Experimental Section

Materials. Grade 5A raw *Bombyx mori* silk with an average denier of 20.86 was obtained from Fiaçào de Seda Bratac S.S. (Brazil), and gelatin (Type A from porcine skin, 175 bloom) was acquired from Sigma Chemicals. All other chemicals used in this study (see the following section) were purchased from Fisher Scientific or Aldrich Chemicals and used directly without further purification.

Methods. *1. Preparation.* A master batch of amorphous SF solution was prepared according to the dissolution method previously reported by Ha et al.[3] The dried silk was degummed with 0.25% w/v sodium lauryl sulfate and 0.25% w/v sodium carbonate in boiling water (bath ratio of 1:10 w/v). After 1 h, the SF was removed and thoroughly washed in deionized water. The residual sericin fraction was calculated as 0.229. Dried SF (10 wt %) was subsequently dissolved in a 75/25 w/w $Ca(NO_3)_2 \cdot 4H_2O$/MeOH solution. The resultant SF solution was dialyzed in a cellulose membrane tube (MWCO 6000−8000) for 4 days with the deionized water changed daily. The concentration of the dialyzed SF solutions, estimated as 4.2 wt %, was diluted to 4 wt % by adding deionized water to the dialyzed SF solution. Dried G was suspended at a concentration of 4 wt % in deionized water, and the suspension was subsequently dissolved under agitation at 40 °C. The composition of each G/SF blend, denoted by G/SF*W* (where *W* denotes the weight percent of G in the blend), was controlled by isothermally mixing predetermined quantities of the parent G and SF solutions. Corresponding films were prepared by solvent casting the G/SF solutions on polystyrene Petri dishes at 10 °C, followed by storage under vacuum at ambient temperature for 1 week. The resultant clear, colorless, and flexible films measuring ca. 200 μm thick were treated with a 75/25 w/w MeOH/water solution for up to 600 min at 20 °C to induce SF crystallization in the presence of the G triple-helix conformation and then dried under vacuum at ambient temperature for 24 h.

2. Analysis. Fourier-transform infrared (FTIR) spectra of all the blends examined here were collected using a Nicolet 510P spectrometer equipped with the attenuated total reflectance (ATR) accessory. All scans were repeated an average of 32 times at a resolution of 4 cm^{-1}. Wide-angle X-ray diffractometry (WAXD) was conducted on representative specimens before and after MeOH treatment with a Siemens Type F diffractometer using Ni-filtered Cu Kα radiation and operated at 35 kV and 25 mA. All scans extended from 5° to 40° in 2θ. Differential scanning calorimetry (DSC) was performed on selected specimens before and after MeOH treatment using a Perkin-Elmer Diamond calorimeter equipped with an intercooler. Thermograms of air-dried films were obtained under an inert nitrogen atmosphere from 25 to 150 °C at a heating rate of 20 °C/min. Thermal gravimetric analysis (TGA) was conducted to discern the concentration of water in and the thermal degradation signature of select dried specimens. Measurements were performed using a Perkin-Elmer TGA Pyris 1. Samples were heated to 200 °C at a rate of 50 °C/min under nitrogen until the TGA curves reached a plateau, which was presumed to signify complete water removal. The initial moisture content was determined from the weight difference between the starting mass and the plateau mass at 200 °C. Samples were subsequently subjected to additional heating to 600 °C to identify the thermal degradation temperature.

The morphological characteristics of the pure SF and G/SF25 blends before and after MeOH treatment were investigated by confocal laser scanning microscopy (CLSM). Dried films were exposed to Alexa Fluor 488 (carboxylic acid succinimidyl ester), an amine-selective fluorescent dye,[25] obtained from Molecular Probes. Fluorescence and differential interference contrast (DIC) images were acquired with a Leica TCS SP confocal microscope illuminated with an Ar laser operated at a wavelength of 488 nm with a fluorescein isothiocyanate filter. Secondary-electron images of film surfaces and cross-sectional fractures produced in liquid nitrogen (sputter-coated with a thin layer of Au to reduce the extent of charging) were collected on a Hitachi S-3200N microscope operated at an accelerating voltage of 5 kV. Extensional rheometry was performed using an INSTRON 5544 instrument equipped with a tension cell of 100 N. Specimens measuring 50 mm long and 6 mm wide were examined at a crosshead speed of 2 mm/min and a gauge length of 20 mm at ambient temperature. The thickness of each sample was taken as the average of seven measurements. To ensure comparable relative humidity (RH) history, the samples were stored for 3 weeks in homemade proximity equilibration cells, wherein the RH was maintained at 75.9 ± 1.3% by utilizing a saturated NaCl solution to regulate the water vapor pressure above the films. The results presented here were averaged over five independent tests.

Results and Discussion

Molecular Reorganization. The transition of regenerated SF films from random coil back to β sheet has been reported[3] after post-treatment with organic solvents such as methanol, ethanol, and 2-propanol. This conformational change might arise as a consequence of SF dehydration, resulting in the reorganization of SF molecules as they endeavor to form intra/intermolecular secondary bonds. In this case, solvent-induced SF crystallization in G/SF blends may be physically hindered due to topological constraints imposed by entanglements with G molecules.[26] To discern if this is the case, we first examine the effect of MeOH treatment time on SF crystallization. The FTIR spectra of as-cast and MeOH-treated SF collected after exposure times of up to 600 min are presented in Figure 1a. Included in this figure is the FTIR spectrum of spun SF fiber, which exhibits the reported[2,27] signature of the β-sheet conformation (silk II structure) at each amide peak: amide I (1625 cm^{-1}), amide II (1520 cm^{-1}), and amide III (1265 cm^{-1}). The amide I peak, which reflects the stretching of C═O groups along the SF backbone, is shifted from 1655 to 1625 cm^{-1}, whereas the amide II peak, which originates from N−H deformation in the SF amide groups, shifts from 1545 to 1520 cm^{-1} at all treatment times. Moreover, in the spectra corresponding to only the MeOH-treated SF films, a new amide III peak arises as a shoulder at 1265 cm^{-1} (with constant intensity) due to vibrations involving the O−C−O and N−H functionalities. While the regenerated (untreated) SF film does not show any evidence of β-sheet structure in its FTIR spectrum, all the films treated with aqueous MeOH from 5 to 600 min exhibit the absorption bands characteristic of the β-sheet structure (see above). The data provided in Figure 1a therefore indicate that virtually all of the solvent-induced transformation from random-coil to β-sheet conformation occurs during the first 5 min of solvent exposure.

In contrast, G films reveal no peak shift in their FTIR spectra after exposure to aqueous MeOH for 2 h at 20 °C (cf. Figure 1b). In this case, the FTIR spectra possess strong absorption bands at 1645 and 1555 cm^{-1}, corresponding to the amide I and amide II peaks, respectively. This result provides evidence that the MeOH treatment has little, if any, effect on G, in agreement with our previous G/SF hydrogel studies.[23] To ascertain if the presence of G influences solvent-induced SF crystallization, we have investigated the FTIR signature of a G/SF60 blend. According to the data displayed in Figure 1c, the as-cast (untreated) film consists of SF molecules exhibiting the random-coil conformation with the amide I and amide II

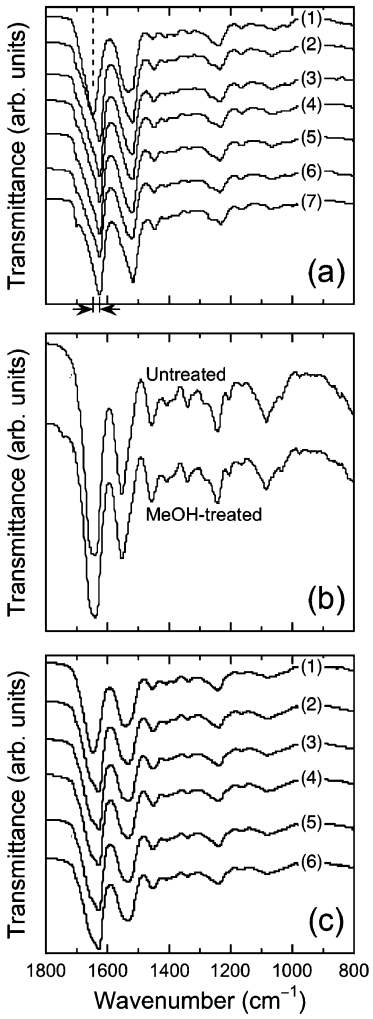

Figure 1. (a) FTIR spectra of pure SF films treated in aqueous MeOH for different times (in min) at 20 °C: (1) 0 (as-cast), (2) 5, (3) 20, (4) 60, (5) 120, and (6) 600. The spectrum labeled (7) corresponds to spun SF fiber. (b) FTIR spectra of G films initially cast from solution and upon exposure to aqueous MeOH for 120 min at 20 °C. (c) FTIR spectra of G/SF60 films treated in aqueous MeOH for the same times as in (a). The spectra in all parts have been vertically shifted to facilitate examination, and the dashed line in (a) identifies the position of the amide-I peak in amorphous SF. The arrows illustrate the shift in the amide-I peak upon exposure to aqueous MeOH and SF crystallization.

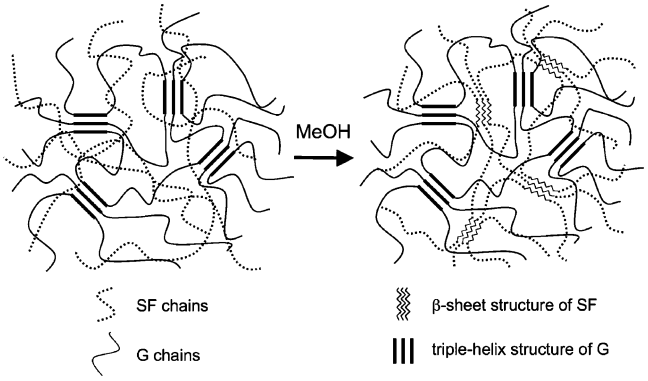

Figure 2. Schematic illustration depicting the effect of MeOH treatment on G/SF blends at 20 °C, which is below the thermally reversible helix-to-coil transition of G. In this scenario, G chains possessing a triple-helix structure are mixed with SF chains to form an initially homogeneous blend. Exposure to aqueous MeOH promotes the crystallization of SF into β sheets, thereby producing a protein blend with two coexisting nanostructures.

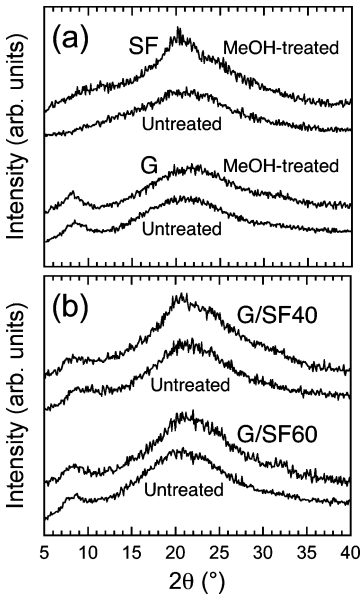

Figure 3. WAXD patterns of (a) pure SF and G, as well as (b) the G/SF40 and G/SF60 blends, before and after exposure to aqueous MeOH for 2 h at 20 °C.

peaks located at 1650 and 1550 cm^{-1}, respectively. Note that the amide III peak in the vicinity of 1270 cm^{-1} is completely absent. It is important to note at this junction that the amide I and amide II peaks observed in this spectrum lie between those of as-cast SF (1655 and 1545 cm^{-1}, respectively) and those of as-cast G (1645 and 1555 cm^{-1}, respectively). When blended polymers are thermodynamically compatible and intermolecular interactions prevail, the resultant FTIR spectra of the blends differ from those of the constituent polymers. Conversely, blends of two incompatible (phase-separated) polymers yield FTIR spectra in which the spectra of the two polymers are superimposed. The FTIR result evident in Figure 1c strongly suggests that these two proteins prior to MeOH treatment are compatible and, thus, mixed at the molecular level. In the remaining FTIR spectra included in this figure, all the blends treated for different times with aqueous MeOH show the absorption bands associated with the β-sheet conformation of SF: 1628 cm^{-1} (amide I), 1530 cm^{-1} (amide II), and 1267 cm^{-1} (amide III). These results are comparable to those obtained from pure SF (cf. Figure 1a) and confirm that the presence of G (with its triple-helix structure at 20 °C) does not hinder the MeOH-induced transformation of SF from random-coil to β-sheet conformation. This result, schematically depicted in Figure 2, implies that relatively short MeOH treatment times are required to induce SF crystallization in G/SF blends. In subsequent sections, the time of specimen exposure to aqueous MeOH is fixed at 2 h.

Another consequence of SF molecular reorganization into β sheets is the onset of crystalline registry, which can be detected by WAXD. Representative WAXD patterns of the pure SF and G polymers before and after aqueous MeOH treatment are presented in Figure 3a, whereas those acquired from the intermediate G/SF40 and G/SF60 blends are provided in Figure 3b. A broad peak centered at $2\theta = 20°$ in the regenerated (untreated) SF has been previously reported[3] as the signature of amorphous SF. A major peak located at $2\theta = 21°$ and two minor peaks at $2\theta = 9°$ and 24°, on the other hand, agree with the assigned peaks of the β-sheet crystalline structure. In Figure 3a, the MeOH-treated SF exhibits a strong WAXD peak at $2\theta = 21°$ and two less intense peaks at $2\theta = 9°$ and 24°, confirming the existence of solvent-induced β crystals. Untreated SF,

however, is characterized by an amorphous diffraction pattern. The two WAXD patterns also displayed for as-cast and MeOH-treated G in Figure 3a are virtually identical, further indicating that the triple-helix structure of G is unaffected by exposure to aqueous MeOH. In Figure 3b, the WAXD patterns collected from the untreated G/SF40 and G/SF60 blends do not show the characteristic peaks associated with crystalline SF. Instead, a single scattering peak evident at $2\theta = 7.8°$ indicates that only the triple-helix structure of G is present in these two untreated blends.[28] Upon exposure to aqueous MeOH, the structure of both blends transforms, as evidenced by the development of scattering peaks located at $2\theta = 21°$ and 24°. This result confirms that the SF conformational transition from random coil to β crystal occurs in the presence of G and that the triple-helix structure of G (i) remains unaffected by exposure to aqueous MeOH and (ii) does not constrain the SF chains as they undergo their solvent-induced conformational change.

Morphological Evolution. Analysis of the FTIR and WAXD data provided in the previous section has established that exposure of regenerated (as-cast) SF and G/SF blends to MeOH post-treatment promotes the formation of SF β crystals. In this section, we investigate the accompanying morphological changes at supramolecular length scales. A previous study by Putthanarat et al.[29] has used green fluorescent protein (GFP) to examine the morphological characteristics of silk extracted directly from different parts of the silk gland in *Bombyx mori*. Near the section of the gland where the silk is synthesized, they find discrete particles measuring ca. 10−20 μm in diameter, as well as some larger irregular-shaped features (which may reflect the presence of different silk structures). Closer to the spinneret, the silk structure evolves to become more continuous and increases in size scale. In addition, fluorescence spectroscopy has been used by Yang et al.[30] to explore the random-coil to β-sheet transition of SF regenerated from ethanol. Their efforts, using anilino-naphthalene-8-sulfonic acid magnesium salt (ANS) as the fluorescent probe, demonstrate that the tryptophan residues of SF become more homogeneously distributed upon SF crystallization and that sorbed water within regenerated SF plays an important role in the conformational transition of SF from random coil to β sheet.

In the present study, Alexa Fluor 488 is used as the fluorescent dye due, in part, to its amine selectivity, since G and SF molecules differ in their amine constitution (ca. 8 and 0.8 mol % for lysine and arginine residues, respectively). Attempts to identify the existence of crystalline structure in as-cast SF, as well as the corresponding G/SF25 blend, by CLSM have been repeatedly unsuccessful, suggesting that as-cast SF is amorphous and that the SF and G molecules are mixed at the molecular level, in agreement with the FTIR and WAXD results reported in the previous section. Figure 4 shows a series of CLSM images acquired from SF (Figure 4a,b) and the G/SF25 blend (Figure 4c) after exposure to aqueous MeOH for 2 h at 20 °C. The matched fluorescent and DIC images in Figure 4, parts a and b, respectively, reveal the existence of long branches measuring on the order of 1−2 μm across. Their dark appearance in Figure 4a is consistent with crystalline structure, which is expected to be impermeable to the fluorescent probe. The DIC imaging mode most clearly shows the evolved SF structure in Figure 4b and is used to examine the MeOH-treated G/SF25 blend in Figure 4c. Comparably branched structures, presumed to constitute SF β crystals, are again evident and measure up to several hundreds of micrometers in length. It is important to recognize that these branched crystals remain visible in both fluorescence and DIC images (data not shown)

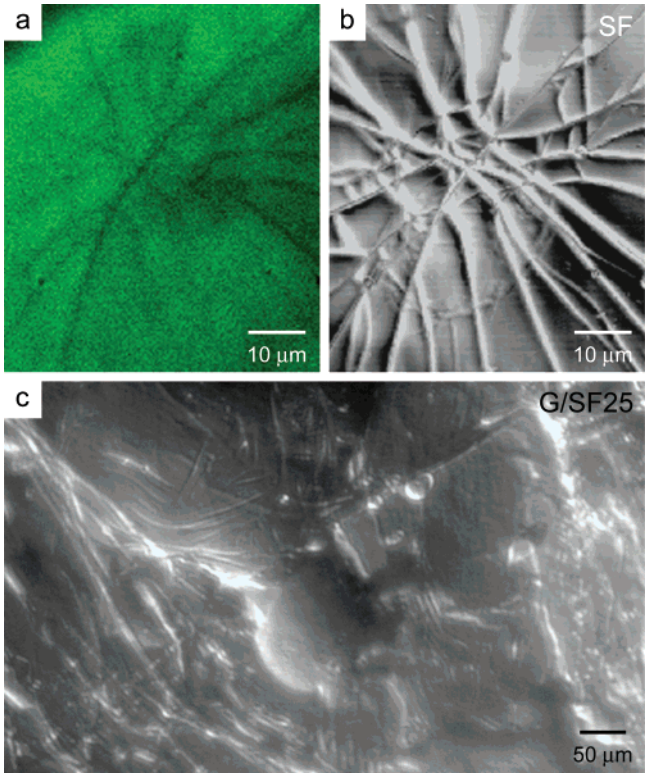

Figure 4. CLSM images acquired from (a,b) pure SF and (c) the G/SF25 blend after exposure to aqueous MeOH for 2 h at 20 °C. The image in (a) has been obtained with a fluorescent dye, whereas the matched image in (b), as well as the one displayed in (c), employs differential interference contrast (DIC).

upon subsequent specimen immersion in phosphate buffer solution, which is used to generate the G/SF hydrogels reported[24] earlier. The CLSM images provided in Figure 4 therefore confirm the development of crystalline structure in regenerated SF and its blends with G upon exposure to aqueous MeOH.

Scanning electron microscopy (SEM) images of the as-cast film surfaces of the G/SF25 and G/SF75 blends prior to aqueous MeOH treatment appear completely featureless, and the corresponding cross-sections generated by fracturing the films in liquid nitrogen show only slight roughness. These characteristics at macroscopic dimensions are again consistent with our earlier findings in this study that untreated G/SF blends are molecularly mixed without any evidence of macrophase separation. This result corroborates our postulated molecular arrangement illustrated in Figure 2, in which amorphous SF molecules are uniformly entangled with G molecules despite the presence of triple helices. Images collected from the same blends after aqueous MeOH treatment for 2 h at 20 °C reveal a profound morphological change. In Figure 5a, the surface of the G/SF25 blend remains flat and featureless, but the visible cross-sectional area exhibits much more topographical detail than the corresponding image of the untreated blend provided in Figure 5b. A dedicated cross-sectional image of the blend is included in Figure 5b and shows a terraced morphology that is representative of crystalline order. The terrace height is estimated to be approximately 300−500 nm. This cross-sectional morphology, which is similar to that observed in pure SF after MeOH treatment (data not shown), is not seen, however, in the G/SF75 blend. Included in Figure 5 are SEM images of the G/SF75 film surface (Figure 5c) and cross section (Figure 5d), which clearly demonstrate that this G-rich blend is not nearly as affected by aqueous MeOH treatment as the SF-rich G/SF25 blend in Figure 5, parts a and b. In fact, parts c and d of Figure

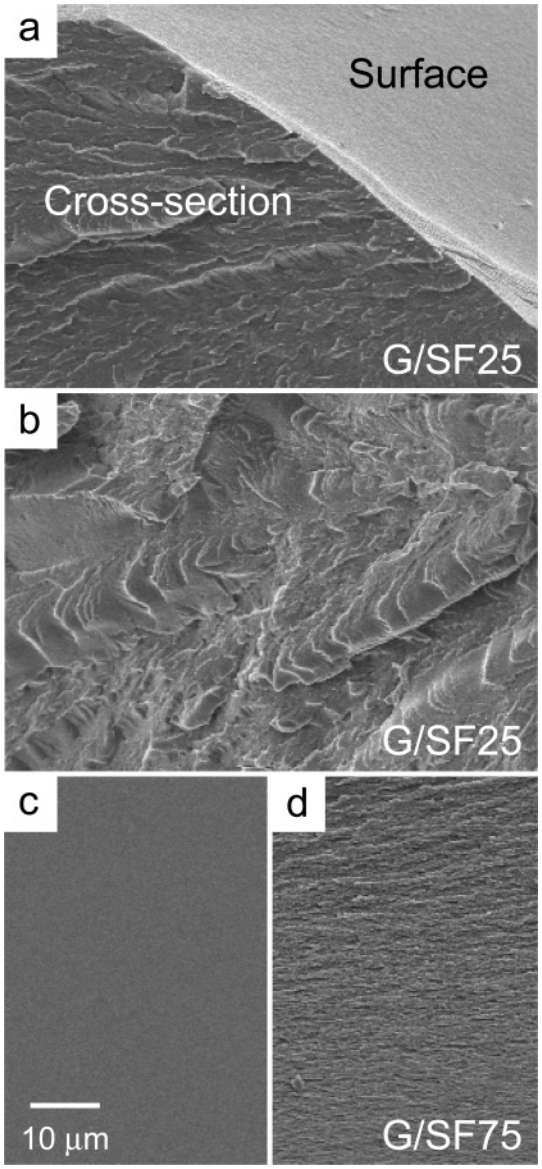

Figure 5. SEM images of MeOH-treated (a,b) G/SF25 and (c,d) G/SF75 blends showing the film surfaces in (a) and (c), as well as their fractured cross sections in (a), (b), and (d). Note that the SF-rich blend exhibits a terraced cross section in (b), which is indicative of crystalline order.

5 closely resemble the featureless as-cast films of the G/SF25 and G/SF75 blends. As before, the absence of macroscopic phase separation in both blends confirms that amorphous SF and G remain highly compatible due to their polypeptide chemistry even after SF crystallization and likewise suggests that the two proteins form IPNs in their blends. This latter aspect is an important consideration if these blends are to be developed as the precursor materials to physically cross-linked hydrogels.[23,24]

Thermomechanical Properties. The thermal properties of proteins such as SF and G are very sensitive to moisture, which acts as a plasticizing agent to depress thermal transition temperatures. Agarwal et al.,[31] for instance, have provided evidence that the glass transition temperature (T_g) of regenerated SF films can be shifted from 178 to 39 °C if the moisture content is increased to 18 wt %. The T_g of G is likewise found to decrease dramatically, from 217 °C for dry G to 0 °C for G with 25 wt % moisture.[32] All the G/SF blends prepared here contain residual moisture at atmosphere conditions. Figure 6a displays DSC thermograms of regenerated (untreated) SF and

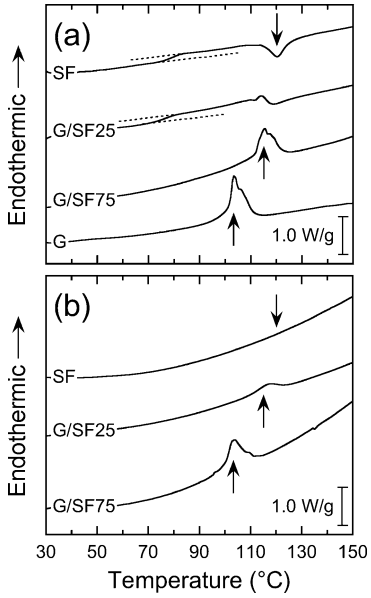

Figure 6. DSC thermograms of pure and blended materials (labeled) (a) before and (b) after aqueous MeOH treatment for 2 h at 20 °C. Residual water concentrations (in wt %) in the untreated specimens are measured to be 8.2 (SF), 9.1 (G/SF25), 10.4 (G/SF75), and 13.4 (G). After MeOH treatment, these concentrations become 5.6, 8.3, and 12.3, respectively (G is not included in this series since it is unaffected by MeOH).

G, as well as the G/SF25 and G/SF75 blends. Corresponding heating curves for MeOH-treated SF and the two blends (G is not included since it is unaffected by aqueous MeOH) are included for comparison in Figure 6b. The moisture content in these blends, as discerned by TGA measurements (see the Experimental Section), is ~10 wt % (measured concentrations are listed in the caption of Figure 6). In Figure 6a, the T_g of air-dried as-cast SF is ~79 °C, which is 82 °C lower than that of fully dried SF (181 °C, as previously reported[3]). Assuming that the T_g behavior of hydrated SF obeys the Fox−Flory equation in conjunction with the data of Agarwal et al.,[31] we predict that amorphous SF with 8.2 wt % water (see the caption of Figure 6) should have a T_g of ~102 °C, which is higher than the value of T_g extracted from Figure 6a. The DSC signature of untreated SF also reveals the existence of a crystallization temperature (T_c) at 120 °C. In fully dried amorphous SF, T_c has been measured[3] to be about 227 °C. Upon exposure to aqueous MeOH for 2 h at 20 °C (Figure 6b), the T_g and T_c signatures of SF are no longer evident over the temperature range investigated. Air-dried G containing 13.4 wt % water exhibits its helix-to-coil transition temperature (T_h) at 103 °C in Figure 6a. The close proximity of this transition to the normal boiling point of water merits discussion.

Water acts to plasticize a wide variety of hydrophilic polymers, including, but not limited to, poly(vinyl alcohol),[33] poly(vinyl pyrrolidone),[34] poly(acrylic acid),[35] and G.[36] In these reports, free water does not crystallize below a critical concentration, and noncrystalline bound water serves as a plasticizer to reduce the T_g of the host polymer. In an aqueous environment, G molecules require the presence of water to form the triple-helix crystal structure, and the resultant mixed crystal exhibits eutectic melting behavior with bound water, despite the large (~230 °C) difference between the normal melting points of pure G and pure water.[36] As in pure SF and G, residual moisture in the G/SF blends is responsible for shifting all the phase transitions to lower temperatures. Generally speaking, the residual water content in G/SF blends increases with increasing

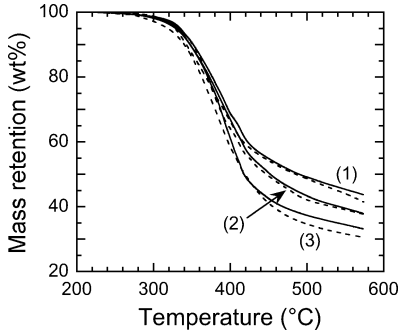

Figure 7. TGA thermograms of (1) pure SF, (2) the G/SF25 blend, and (3) the G/SF75 blend before (dashed lines) and after (solid lines) exposure to aqueous MeOH for 2 h at 20 °C.

Table 1. Degradation Characteristics Obtained from Thermal Gravimetric Analysis of SF, G, and Their Blends with and without MeOH Post-treatment

system	MeOH-treated[a]	onset temp (°C)	max rate (MR) (%/°C)	MR temp (°C)	residue (%) at 380 °C	residue (%) at 550 °C
SF	no	323	0.39	377	74.8	44.0
G/SF25	no	334	0.43	373	74.0	39.0
G/SF75	no	331	0.50	379	70.3	31.6
G	no	340	0.52	378	73.4	31.4
SF	yes	337	0.47	392	78.5	45.3
G/SF25	yes	342	0.59	388	76.8	39.7
G/SF75	yes	348	0.60	391	75.1	34.4

[a] Immersion in 75/25 w/w MeOH/water for 2 h at 20 °C.

G concentration, which reflects the greater hydrophilicity of G relative to SF. In the G/SF25 blend, the T_g of SF remains visible at 76 °C in Figure 6a. At higher temperatures, the exothermic peak corresponding to the T_c of SF (at 119 °C) is observed to merge into the endothermic peak corresponding to the T_h of G (114 °C). While possibly serendipitous, this result is intriguing since these transitions for fully dried pure SF and G are surprisingly close (220−230 °C).[3,36] Increasing the concentration of G to 75 wt % in the untreated G/SF75 blend (cf. Figure 6a) completely eliminates detection of the T_g and T_c transitions associated with SF. Conversely, the T_h of G is pronounced and remains at nearly the same temperature (115 °C) as in the G/SF25 blend. Exposing the G/SF blends described in regard to Figure 6a to aqueous MeOH for 2 h at 20 °C yields the results displayed in Figure 6b. The thermal transitions of SF are entirely absent over the temperature range probed, which further supports our contention that aqueous MeOH treatment promotes SF crystallization in G/SF blends, as well as in pure SF. The helix-to-coil transition of G is evident in the thermograms acquired from the two G/SF blends under examination. The pronounced shift in T_h of the G/SF75 blend to 103 °C most likely reflects the increased moisture content in this MeOH-treated blend (12.3 wt %) relative to its untreated analogue (10.4 wt %).

The thermal stability of pure SF and G, as well as their blends, before and after aqueous MeOH treatment has also been investigated, and representative TGA thermograms are presented in Figure 7. Two degradation regimes are apparent: one related to the decomposition of side chain functionalities between 300 and 420 °C, and the other corresponding to decomposition of the protein backbone at temperatures above 420 °C. The degradation onset temperature, maximum degradation rate, and temperature at the maximum degradation rate are metrics related to the first degradation regime, and their values are compiled in Table 1. While the onset temperature does not correlate with blend composition, one apparent tendency is noteworthy: exposure of pure SF or a G/SF blend to aqueous MeOH increases the degradation onset temperature (by as much as 17 °C in the G/SF75 blend). This result can be explained in terms of β-sheet formation. When the SF chains adopt the β-sheet conformation, intermolecular secondary bonds (parallel hydrogen bonding and van der Waals forces) protect the side chain functionalities of SF by increasing the activation energy required to break their covalent bonds. Another interesting result evident in Table 1 is that the onset temperature of gelatin (340 °C) is closer to that of MeOH-treated SF (337 °C) than that of untreated SF (323 °C). This observation is likewise presumed to be a consequence of supramolecular organization, since the triple-helix structure of G promotes crystalline order[37] much in the same fashion as the β crystals in SF. The maximum degradation rate and its corresponding temperature are also influenced by molecular conformation. After MeOH treatment, all the SF-containing specimens exhibit substantial increases in both metrics, signifying that (i) the degradation mechanism occurs more abruptly at higher temperature and (ii) resistance increases against molecular degradation induced by thermal energy. In short, these results confirm that the thermal stability of SF improves with increasing crystalline order due to the formation of protective secondary bonds. An unexpected result in Table 1 is that the degradation onset temperature and maximum degradation rate of the MeOH-treated G/SF blends are consistently higher than those of MeOH-treated SF and G. While this trend suggests that the two crystalline networks act synergistically to resist thermal degradation, more work is required to elucidate the molecular-level mechanism responsible for this observation.

Another aspect of Figure 7 that warrants discussion is the mass retention (or residue) within the two degradation regimes. In the first regime, we have selected a reference temperature of 380 °C, since it approximates the average temperature corresponding to the maximum degradation rate for all the specimens examined (383 °C). The reference temperature in the second regime is arbitrarily chosen to be 550 °C. Values of the residues measured at these two temperatures are included in Table 1. At both temperatures, three trends can be identified. The first is that MeOH-treated SF possesses the highest residue at both reference temperatures, which suggests that the secondary interactions associated with the β-sheet conformation provide improved thermal stability at high temperatures relative to the random-coil conformation of SF or the triplex-helix structure of G. In this same vein, the second trend to warrant mention is that SF crystallization consistently increases the residue of all SF-containing specimens at both reference temperatures. The MeOH-induced change in residue is more profound at 380 °C (3.8% on average) than at 550 °C (1.6% on average), confirming that the conformational change of SF enhances the thermal stability of SF and its blends with G more in the first degradation regime (wherein the side groups of proteins rapidly degrade) than in the second regime (wherein the protein backbone degrades). This conclusion supports the molecular reorganization conclusions reached by Yang et al.[30] in their fluorescence spectroscopy studies of solvent-induced SF crystallization. The third trend evident in Table 1 is that, upon MeOH treatment, the residue decreases monotonically with increasing G concentration. This result can be interpreted by considering the difference in the chemical constitution of the two proteins. The SF chains consist mainly of amino acid units with short side groups such as glycine and alanine,[38] whereas G is primarily composed of amino acids with longer side groups such as proline

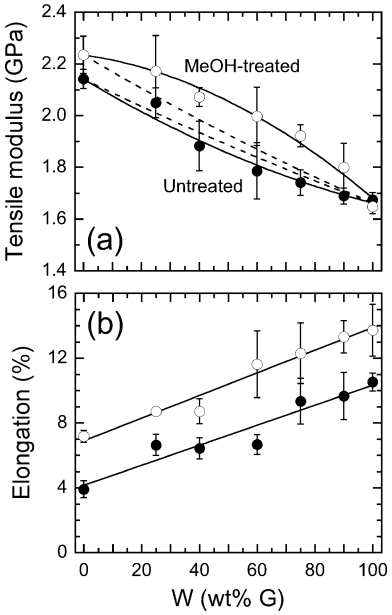

Figure 8. Dependence of (a) tensile modulus and (b) elongation on composition (W) in G/SF blends with (○) and without (●) post-MeOH treatment. The solid lines in (a) serve as guides for the eye, whereas those in (b) are linear regressions to the data. The dashed lines in (a) represent predictions from the rule of mixtures (eq 1). The error bars denote the standard error in the data.

and hydroxyproline.[37] On the basis of these considerations and the TGA data provided in Table 1, it follows that the more compact side groups on the SF chains located within the protected confines of β sheets are less susceptible to thermal degradation than the longer and more exposed bulkier side groups on the G chains. Because of their increased mass, degradation of the side groups on the G chains results in greater overall mass loss and, hence, a reduction in residue relative to that of SF.

The mechanical properties addressed in this study are determined by uniaxial tensile deformation performed at ambient temperature. Values of the tensile modulus (E) for SF, G, and G/SF blends with and without MeOH treatment are presented as a function of blend composition in Figure 8a and reveal that E systematically increases (i) with decreasing G content and (ii) upon MeOH treatment (assuming that MeOH has no effect on pure G, as suggested by previous results reported in this work). If the amorphous SF and G possess comparable densities at ambient temperature, the modulus values measured from the as-cast (untreated) blends are found to be reasonably well represented by the rule of mixtures proposed by Gray and McCrum[39] for unoriented composite polymer systems:

$$\log E = \phi_G \log E_G + \phi_{SF} \log E_{SF} \qquad (1)$$

where ϕ denotes volume fraction (which is equal to weight fraction in the limit of identical mass densities), and E_G and E_{SF} are the tensile moduli of pure G and SF, respectively. Application of eq 1 to the MeOH-treated blends sorely underpredicts the data, suggesting that, upon β-sheet formation, the SF and G networks synergistically influence the resistance of the G/SF blends to deformation. As such, this result supports our earlier observation regarding the resistance of the G/SF blends to thermal degradation. Figure 8b shows the composition dependence of the tensile elongation at failure (or strain at break). An increase in the low-modulus G fraction generally promotes a nearly linear increase in elongation before and after

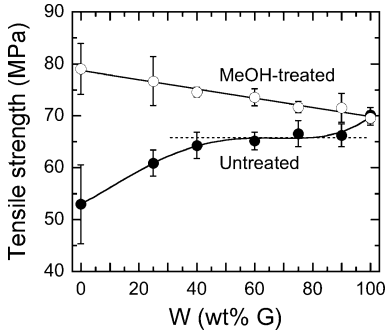

Figure 9. Tensile strength presented as a function of W for G/SF blends with (○) and without (●) post-MeOH treatment. The upper solid line is a linear regression to the data, whereas the lower solid line serves as a guide for the eye. The dotted horizontal line identifies the apparent plateau in the data, and the error bars correspond to the standard error in the data.

MeOH treatment. In contrast to the trends evident in Figure 8a, however, MeOH treatment also yields a systematic shift in elongation to higher values. This increase in elongation is attributed to two factors involved in complex interplay: (i) formation of β crystals that serve to reinforce the matrix and (ii) introduction of water that plasticizes both SF and G. The composition dependence of the tensile strength is displayed in Figure 9 and reveals markedly different behavior before and after MeOH treatment. In the absence of β crystals, SF exhibits the lowest tensile strength of the series. As the concentration of G in the G/SF blends is increased, the tensile strength initially increases, reaches a plateau, and then attains its maximum value (at pure G). Introduction of β crystals following aqueous MeOH treatment, however, results in a linear increase in tensile strength with increasing SF content. It should be noted, however, that the magnitudes of the tensile moduli and tensile strength reported in Figures 8 and 9 are generally lower than those compiled by Altman et al.[40]

Conclusions

The primary objective of the present study has been to ascertain if the solvent-induced conformational transition of regenerated SF from random coil to β sheet could be extended to blends of regenerated SF with another polymer, such as G. The development of such blends would, upon SF crystallization, yield physically cross-linked IPNs in which each constituent species possesses unique molecular organization, since G exhibits a triple-helix structure at ambient temperature. Infrared spectroscopy and X-ray diffraction have been employed here to demonstrate that the crystallization of amorphous SF in binary blends with G occurs quickly, typically within a few minutes, without any noticeable complications. These blends show no sign of macroscopic phase separation before or after exposure to aqueous MeOH. Confocal and electron microscopies confirm the development of crystalline structure in pure SF and G/SF blends once SF undergoes its conformational change to β sheet. Thermal calorimetry reveals the existence of relatively low-temperature thermal transitions (T_g and T_c) in untreated SF and SF-rich blends with G. These transitions disappear entirely upon MeOH treatment due to the formation of β crystals. The helix-to-coil transition of G, however, remains virtually unaffected. Thermal gravimetric analysis also provides evidence to indicate that the formation of the β-sheet structure generally promotes improved thermal stability of pure SF and SF-containing blends at elevated temperatures. Crystallization of SF likewise enhances the mechanical properties, such as tensile modulus, elongation,

and tensile strength, of G/SF blends. The blend strategy developed here and used elsewhere[23,24] to produce physically cross-linked, thermally responsive G/SF hydrogels is based on the crystallizable attributes of SF and is sufficiently general to be extended to blends of SF with synthetic polymers, as well as other biomacromolecules. The results of this study provide the foundation for a novel multicomponent approach wherein SF can be used in conjunction with other self-organizing or crystallizable (bio)polymers to generate (semi)IPNs with multiple structures and, as demonstrated here, synergistic properties. Due to their chemical attributes and inherent physical properties, these blends can serve as the basis for other functionalized materials of interest in the biomedical and pharmaceutical industries.

Acknowledgment. This work was supported by Nexia Biotechnologies Inc. (Vaudreuil-Dorion, Quebec, Canada) and Banner Pharmacaps, Inc. (High Point, NC). We thank Drs. N.S. Allen and E. Johannes for helpful comments and advice regarding the confocal microscopy.

References and Notes

(1) Zhou, C. Z.; Confalonieri, F.; Medina, N.; Zivanovic, Y.; Esnault, C.; Yang, T.; Jacquet, M.; Janin, J.; Duguet, M.; Perasso, R.; Li, Z. G. *Nucleic Acids Res.* **2000**, *28*, 2413.
(2) Mathur, A. B.; Tonelli, A.; Rathke, T.; Hudson, S. M. *Biopolymers* **1997**, *42*, 61.
(3) Ha, S. W.; Park, Y. H.; Hudson, S. M. *Biomacromolecules* **2003**, *4*, 488.
(4) Nazarov, R.; Jin, H. J.; Kaplan, D. L. *Biomacromolecules* **2004**, *5*, 718.
(5) (a) Minoura, N.; Aiba, S.; Gotoh, Y.; Tsukada, M.; Imai, Y. *J. Biomed. Mater. Res.* **1995**, *29*, 1215. (b) Minoura, N.; Aiba, S. I.; Higuchi, M.; Gotoh, Y.; Tsukada, M.; Imai, Y. *Biochem. Biophys. Res. Commun.* **1995**, *208*, 511. (c) Gotoh, Y.; Tsukada, M.; Minoura, N.; Imai, Y. *Biomaterials* **1997**, *18*, 267.
(6) Minoura, N.; Tsukada, M.; Nagura, M. *Polymer* **1990**, *31*, 265.
(7) Gu, J.; Yang, X.; Zhu, H. *Mater. Sci. Eng., C* **2002**, *20*, 199.
(8) Kweon, H. Y.; Um, I. C.; Park, Y. H. *Polymer* **2001**, *42*, 6651.
(9) Yang, G.; Zhang, L.; Liu, Y. *J. Membr. Sci*. **2000**, *177*, 153.
(10) Li, M.; Minoura, N.; Dai, L.; Zhang, L. *Macromol. Mater. Eng*. **2001**, *286*, 529.
(11) Gao, Q.; Shao, Z.; Sun, Y.; Lin, H.; Zhou, P.; Yu, T. *Polym. J*. **2000**, *32*, 269.
(12) Liu, Y.; Shao, Z.; Zhou, P.; Chen, X. *Polymer* **2004**, *45*, 7705.
(13) Digenis, G. A.; Gold, T. B.; Shah, V. P. *J. Pharm. Sci.* **1994**, *83*, 915.
(14) Laemmel, E.; Penhoat, J.; Warocquier-Clérout, R.; Sigot-Luizard, M. F. *J. Biomed. Mater. Res.* **1998**, *39*, 446.
(15) Ulubayram, K.; Cakar, A. N.; Korkusuz, P.; Ertan, C.; Hasirci, N. *Biomaterials* **2001**, *22*, 1345.
(16) (a) Cai, K.; Yao, K.; Lin, S.; Yang, Z.; Li, X.; Xie, H.; Qing, T.; Gao, L. *Biomaterials* **2002**, *23*, 1153. (b) Masuda, T.; Furue, M.; Matsuda, T. *Tissue Eng.* **2004**, *10*, 523.
(17) (a) Joly-Duhamel, C.; Hellio, D.; Djabourov, M. *Langmuir* **2002**, *18*, 7208. (b) Joly-Duhamel, C.; Hellio, D.; Ajdari, A.; Djabourov, M. *Langmuir* **2002**, *18*, 7158.
(18) Olde Damink, L. H. H.; Dijkstra, P. J.; van Luyn, M. J. A.; van Wachem, P. B.; Nieuwenhuis, P.; Feijen, J. *J. Mater. Sci.: Mater. Med.* **1995**, *6*, 460.
(19) (a) Olde Damink, L. H. H.; Dijkstra, P. J.; van Luyn, M. J. A.; van Wachem, P. B.; Nieuwenhuis, P.; Feijen, J. *J. Mater. Sci.: Mater. Med.* **1995**, *6*, 429. (b) Apostolov, A. A.; Boneva, D.; Vassileva, E.; Mark, J. E.; Fakirov, S. *J. Appl. Polym. Sci.* **2000**, *76*, 2041.
(20) Ulubayram, K.; Aksu, E.; Gurhan, S. I. D.; Serbetci, K.; Hasirci, N. *J. Biomater. Sci., Polym. Ed.* **2002**, *13*, 1203.
(21) Bigi, A.; Cojazzi, G.; Panzavolta, S.; Roveri, N.; Rubini, K. *Biomaterials* **2002**, *23*, 4827.
(22) Kuijpers, A. J.; Engbers, G. H. M.; Feijen, J.; De Smedt, S. C.; Meyvis, T. K. L.; Demeester, J.; Krijgsveld, J.; Zaat, S. A. J.; Dankert, J. *Macromolecules* **1999**, *32*, 3325.
(23) Gil, E. S.; Spontak, R. J.; Hudson, S. M. *Macromol. Biosci.* **2005**, *5*, 702.
(24) Gil, E. S.; Frankowski, D. J.; Spontak, R. J.; Hudson, S. M. *Biomacromolecules* **2005**, *6*, 3079.
(25) Panchuk-Voloshina, N.; Haugland, R. P.; Bishop-Stewart, J.; Bhalgat, M. K.; Millard, P. J.; Mao, F.; Leung, W.-Y.; Haugland, R. P. *J. Histochem. Cytochem*. **1999**, *47*, 1179.
(26) For a similar physical situation, see, for example: Walker, T. A.; Melnichenko, Y.; Wignall, G. D.; Lin, J. S.; Spontak, R. J. *Macromol. Chem. Phys*. **2003**, *204*, 2064 and references therein.
(27) Viney, C. *J. Text. Inst*. **2000**, *91*, 2.
(28) (a) Bigi, A.; Cojazzi, G.; Panzavolta, S.; Rubini, K.; Roveri, N. *Biomaterials* **2001**, *22*, 763. (b) Bigi, A.; Panzavolta, S.; Rubini, K. *Biomaterials* **2004**, *25*, 5675.
(29) Putthanarat, S.; Eby, R. K.; Naik, R. R.; Juhl, S. B.; Walker, M. A.; Peterman, E.; Ristich, S.; Magoshi, J.; Tanaka, T.; Stone, M. O.; Farmer, B. L.; Brewer, C.; Ott, D. *Polymer* **2004**, *45*, 8451.
(30) Yang, Y.; Zhengzhong, S.; Chen, X.; Zhou, P. *Biomacromolecules* **2004**, *5*, 773.
(31) Agarwal, N.; Hoagland, D. A.; Farris, R. J. *J. Appl. Polym. Sci.* **1997**, *63*, 401.
(32) Rose, P. I. In *The Theory of the Photographic Process*, 4th ed.; James, T. H., Ed.; MacMillan: New York, 1977; p 67.
(33) Rault, J.; Gref, R.; Ping, Z. H.; Nguyen, Q. T.; Néel, J. *Polymer* **1995**, *36*, 1655.
(34) Rault, J.; Gref, R.; Ping, Z. H.; Nguyen, Q. T. *J. Non-Cryst. Solids* **1994**, *172*, 733.
(35) Ponomariova, T.; Melnichenko, Y.; Albouy, P. A.; Rault, J. *Polymer* **1997**, *38*, 3561.
(36) Patil, R. D.; Mark, J. E.; Apostolov, A.; Vassileva, E.; Fakirov, S. *Eur. Polym. J.* **2000**, *36*, 1055.
(37) Nijenhuis, K. *Thermoreversible Networks: Viscoelastic Properties and Structure of Gels*; Springer: Berlin, 1997; pp 160−193.
(38) Suzuki, Y.; Gage, L. P.; Brown, D. D. *J. Mol. Biol.* **1972**, *70*, 637.
(39) Gray, R. W.; McCrum, N. G. *J. Polym. Sci., Part A-2* **1969**, *7*, 1329.
(40) Altman, G. H.; Diaz, F.; Jakuba, C.; Calabro, T.; Horan, R. L.; Chen, J.; Lu, H.; Richmond, J.; Kaplan, D. L. *Biomaterials* **2003**, *24*, 401.

BM050622I